TOPOLOGY PROCEEDINGS

Volume 44, 2014

Pages 257–284

http://topology.auburn.edu/tp/

Modeling a Chaotic Machine's Dynamics as a Linear Map on a "Square Sphere"

by

J. T. Halbert and James A. Yorke

Electronically published on November 25, 2013

Topology Proceedings

Web:	http://topology.auburn.edu/tp/
Mail:	Topology Proceedings
	Department of Mathematics & Statistics
	Auburn University, Alabama 36849, USA
E-mail:	topolog@auburn.edu
ISSN:	0146-4124

http://topology.auburn.edu/tp/
TOPOLOGY PROCEEDINGS
Volume 44 (2014)
Pages 257-284
E-Published on November 25, 2013

MODELING A CHAOTIC MACHINE'S DYNAMICS AS A LINEAR MAP ON A "SQUARE SPHERE"

J. T. HALBERT AND JAMES A. YORKE

Abstract. We create models of a taffy pulling machine and display them via animation. We describe the action of this machine and first model its discrete-time dynamics with a family of chaotic maps on the interval $[0, 1]$. Further abstraction leads to a second model, an area-preserving map on a region of the plane. From this latter representation we proceed to a third model, a map on what we call the "square sphere." This map is pseudo-Anosov. Our animations help mathematicians visualize our models and we extend this approach to the Plykin, Newhouse, and baker's maps. We also show a related process that is modeled on what we call a "triangular sphere."

1. Introduction

A taffy pulling machine is used to create sugary, chewy candy called "taffy" or "salt water taffy." The machine's periodic motions (Figure 1) are so mesmerizing that, when placed in a store window, it attracts audiences. The consistent stretching of the candy suggests chaotic dynamics. Because of this, a taffy pulling machine has often been used informally as an example of such behavior, e.g., in [8]. The goal of this paper is to present intriguing models of an idealized taffy pulling machine, or more precisely, the discrete-time, one-period motion. (See figures 2 and 3.)

2010 *Mathematics Subject Classification.* 54X10, 58Y30, 18D35; Secondary 55Z10.

Key words and phrases. geometry, low dimensional dynamical systems, mechanics of deformable solids, topological dynamics.

The research for the first author was supported under a National Defense Science and Engineering Graduate Research Fellowship.

The research for the second author was supported under National Science Foundation grant DMS-0616585.

Viewed electronically, this paper makes use of animation to show how the idealized taffy pulling machine is related to abstract chaotic dynamical processes. We believe animation greatly aids understanding, but it is not necessary for understanding. Readers of the print version should find more than enough details to edify. **The message "click on image" in some figures is intended to direct the reader to click an image to view an animation.**

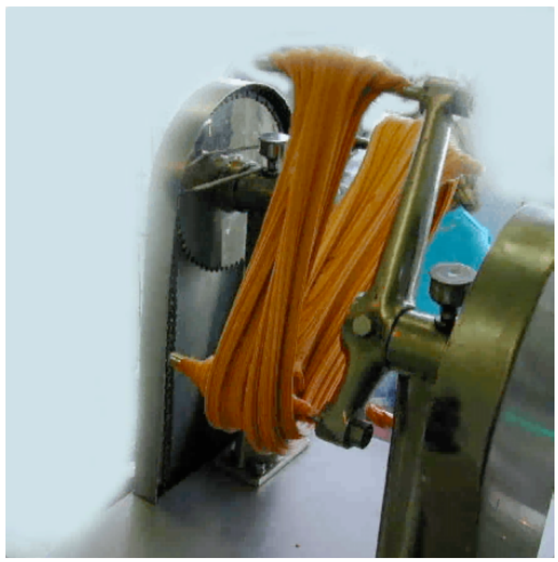

FIGURE 1. Taffy Pulling Machine. [Click on image.]

Figure 3 shows how three colored regions are deformed by the time-1 map. To make this drawing, we chose the length S of the short arm to be 0 (see Figure 5), a choice that we later argue helps create a more uniform stretching of the taffy. The stars denote a period-2 orbit that lies on the surface of the taffy.

Shown below, the baker's map is like the taffy map shown in Figure 2, being one-to-one except on parts of the boundary. Unlike the taffy map, the baker's map is discontinuous (along the horizontal line that divides the square in two).

We take the taffy dynamics and through abstraction produce models of its action. The models are related in spirit to the Plykin map, a diffeomorphism on the plane with a hyperbolic attracting set. Visualizing the dynamics of that map was sufficiently difficult that a slightly less

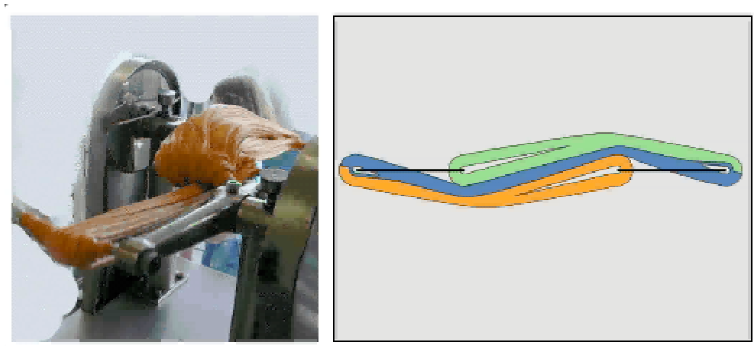

FIGURE 2. Machine and Map. [Click on image.]

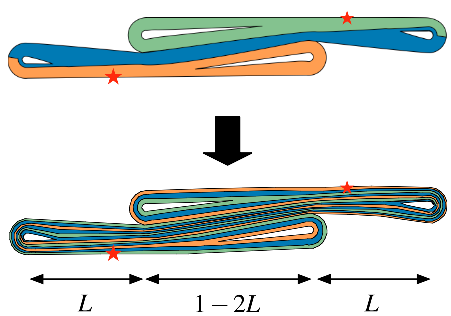

FIGURE 3. Time-1 Map.

challenging map, the Newhouse map, was presented by Clark Robinson [11]. In 2006, Yves Coudene [5] provided some beautiful visualizations of the invariant sets associated with such maps. We turn these discrete-time processes into continuous-time processes to better communicate the dynamics.

Figure 4 and figures 25–27 (see section 8) display our efforts. Because we believe the results presented here may be of interest to students, we have included more details than necessary in some places.

After describing the machine in section 2, we present a continuous piecewise-linear one-dimensional model in section 3. Sections 4–6 investigate the two-dimensional situation.[1]

---

[1]It is clear that the actual taffy-pulling process is three dimensional. However, when viewed from the side, it can be thought of as an area-preserving process in the plane, which is the approach we take.

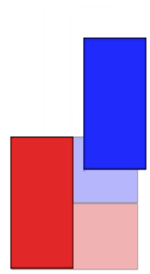

FIGURE 4. Baker's Map. [Click on image.]

2. The Taffy Pulling Machine

Figure 5 shows a schematic drawing of the type of machine we wish to consider. The machine has two independent elements, each of which rotates about a fixed axle, and has two cams (cylinders) on which the taffy hangs. These rotating elements have the same geometry. Let S and L denote the length of the shorter and longer arms, respectively. We chose the horizontal scale so that the total width of the machine in resting position is 1; hence, $S, L \in [0, 1]$. Only certain values of S and L are allowed, however. In order for the machine to work in the manner shown, we must require that $L + S < 1/2$ and $L > 1/4$ (see section 2.1).

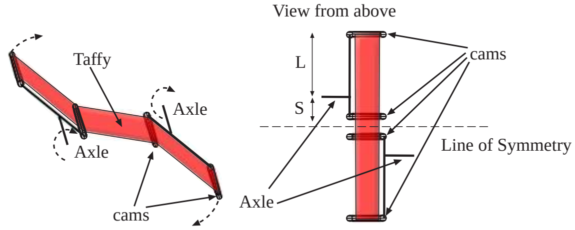

FIGURE 5. Taffy Pulling Machine Schematic.

To focus on the uniform stretching of the taffy, we assume that gravity plays no role and that the taffy is an incompressible two-dimensional linearly elastic material. That is, we assume that all stretching preserves area and is linear between each pair of cams. We scale time so that the period of one full revolution is 1 and we will sometimes refer to the time-1 map as portraying one period of the process.

2.1. Parameter space for taffy pulling machine.

To preserve the topological properties of the taffy time-1 map, we require two features be preserved for the case we are interested in. The gap between the interior cams (Γ in Figure 6) must be positive. This, given that the total length is 1, implies

$$L + S < \frac{1}{2}. \tag{2.1}$$

We must also require that the overlap after 180° suggested in Figure 6 must actually be there. If this overlap were not there, the two rotating elements would not interact and the taffy would be wound around each element until breaking. This implies we need to enforce $L > S + \Gamma/2$ which means we need

$$L > \frac{1}{4}. \tag{2.2}$$

Equations (2.1) and (2.2) give us the region of allowable parameters, shown on the right in Figure 6. The horizontal scale is chosen so that the entire length $(2L + 2S + \Gamma)$ is 1.

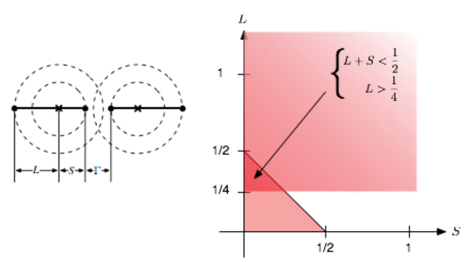

Figure 6. Extended Taffy Pulling Machine Schematic.

3. The 1-D Model

In Figure 7, the mass and area of taffy have been shrunk to one-dimensional curves with branches. To aid visualization, we unrealistically do not merge the layers as the machine moves.

In Figure 8, when we shrink the cams and loops to points and allow merging, we obtain our first model, a continuous time process in the plane. Here, the taffy is a one-dimensional piecewise-linear curve which changes with time. This figure is obtained from Figure 7 by taking the limit as the cams on which the taffy hangs are shrunk toward 0 radius.

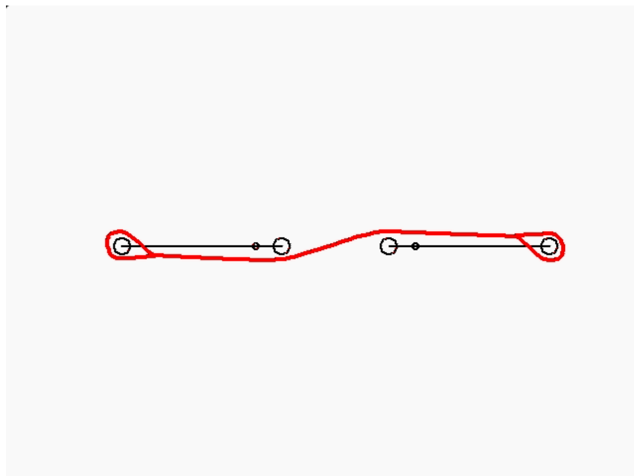

FIGURE 7. One-Dimensional Branched Manifold Version of the Taffy-pulling Process. [Click on image.]

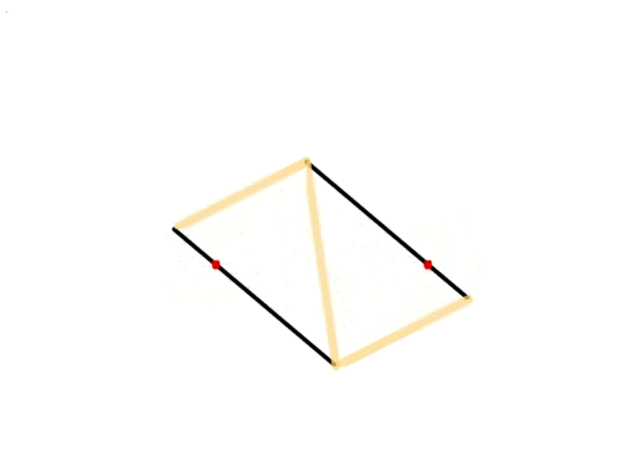

FIGURE 8. Continuous Time 1-D Taffy-pulling Process in the Plane. [Click on image.]

Figure 9 illustrates the piecewise linear maps of the two portions of the taffy motion, each corresponding to a 180° rotation of the axles. T_1 shows the transition from the position where the machine is maximally extended. T_2 begins 180° later, when the machine is minimally extended.

The point r_1 is the location of the left rotation point. The point c_2 is the location of the second cam from the left ($c_1 = 0$ in this image). The point a is the image of the rightmost cam. T_2 shows the return to full extension.

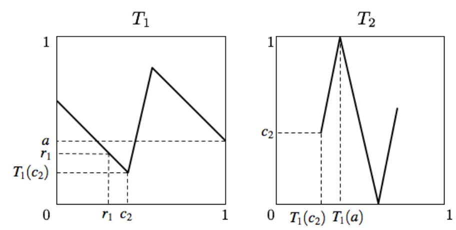

FIGURE 9. Piecewise Linear Maps of the Two Portions of the Taffy Motion.

The time-1 map T is a composition of two processes T_1 and T_2 that describe the movement of the horizontal coordinate of a point in the taffy under rotations of 180°. By analyzing how the various slopes (the absolute value of the derivative) of $T_2 \circ T_1$ (Figure 10) depend on the parameters S and L, we find that there is one and only one choice of S and L for which all the slopes are the same. This happens when $S = 0$ and $L = 1 - \sqrt{2}/2$.

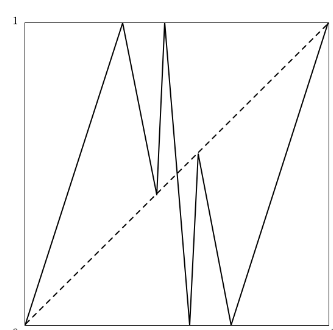

FIGURE 10. Full Piecewise Linear Map of the Taffy-pulling Process.

For this choice, T is defined as follows.

$$T(x) = \begin{cases} \sigma x, & x \in [0, p_1) \\ 2 - \sigma x, & x \in [p_1, p_2) \\ \sigma x - \sqrt{2}, & x \in [p_2, p_3) \\ 2 + \sqrt{2} - \sigma x, & x \in [p_3, 1/2) \\ -T(1-x), & x \in [1/2, 1] \end{cases} \tag{3.1}$$

where

$$\sigma = 3 + 2\sqrt{2} \approx 5.828,$$
$$p_1 = 3 - 2\sqrt{2},$$
$$p_2 = 1 - \frac{\sqrt{2}}{2},$$
$$p_3 = \sqrt{2} - 1\,.$$

Figure 11 is the graph of T, selected so that it has a constant stretch rate σ. Notice there are five fixed points (denoted by dots on the graph): 0, p_2, $1/2$, $1 - p_2$, 1. Physically, these correspond to the x-coordinates of the cams (the outer four of the positions of the cams) and the center point that is demanded by symmetry. T is a piecewise expanding map.

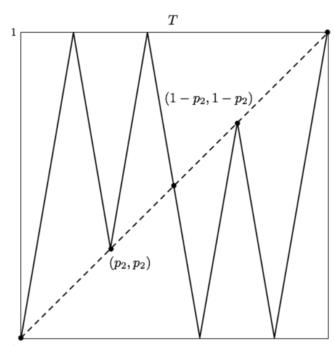

FIGURE 11. The Taffy Map T.

The invariant density. The iteration properties of such maps are well known. For instance, we know there exists an invariant measure (see [1]and [6]) which has a density ρ given by

$$\rho(x) = \begin{cases} \frac{1}{2} + \frac{\sqrt{2}}{4} & x \in [0, L) \cup [1-L, 1] \\ \sqrt{2}\left(\frac{1}{2} + \frac{\sqrt{2}}{4}\right) & x \in [L, 1-L). \end{cases} \tag{3.2}$$

We can view the one-dimensional case as the limit of cases where the taffy is thin and the cams are small. As shown in Figure 12, the density is $\sqrt{2}$ times higher in the middle segment than on the end segments. This information will be important in the next section where we examine the full process in the plane.

The density shows the relative thickness of the taffy rescaled so that $\int_0^1 \rho = 1$. Notice that the integral of ρ from 0 to L or from $1 - L$ to 1 is $\frac{1}{4}$, while the integral over the midsection is $\frac{1}{2}$.

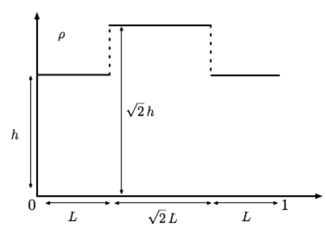

FIGURE 12. Invariant density ρ where $h = \frac{1}{2} + \frac{\sqrt{2}}{4}$ and $L = 1 - \frac{\sqrt{2}}{2}$.

More reality? We note that the map T is independent of the density. It would be more realistic to model the stretching as depending on the density. On each segment between cams, higher density regions would stretch less than lower density ones. However, in all our simulations, the non-uniform taffy refused to converge to steady state and, in effect, broke. Nonetheless, the actual taffy machine works. Since our steady state has constant density between cams, it is also the steady state for the more general dynamics.

4. The 2-D Block Model

In this section, we create a model of the taffy dynamics in two dimensions with an explicit description of the time-1 map. As is often true of models, this model is for a limiting case, the case of very thin taffy.

In Figure 13, each cam is treated as shown on the left: We slice the taffy at each cam and then flatten the two end pieces for each cam, eliminating the cam holes. This process eliminates curvilinear edges. To preserve the original topology, the pairs of points that came from one due to the splitting are identified by semi-circles. We mathematically glue the cut edges back together by identifying the points along the cut edges. Next, we rescale the vertical coordinate to be as high as it is wide, with the cuts becoming vertical edges in the thin-taffy limit, yielding the lower right picture. The four cams become points at the center of the four vertical edges.

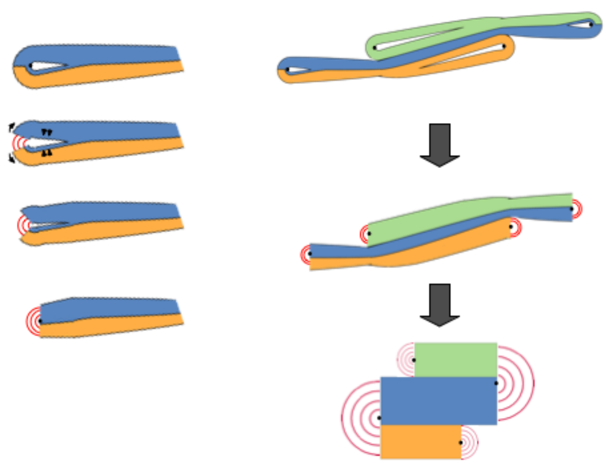

FIGURE 13. Creating the Taffy Block Map.

Figure 14 shows the proportions of the block in the lower right of Figure 13. The dynamics are such that the x coordinate behaves according to the 1-D map T. Points near a cam do not move far from the cam under the time-1 map; hence, in the limit, the cams become fixed points.

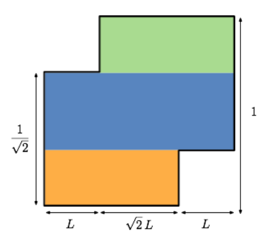

FIGURE 14. The set X, vertically rescaled taffy, where $L = 1 - \frac{\sqrt{2}}{2}$.

This limiting process produces the time-1 map shown in Figure 15. The thickness of the taffy is proportional to the invariant density in section 3. We write X for the subset of the plane shown in Figure 14, and we write $\hat{X}$ for the topological space obtained by making the identifications (the semi-circles in Figure 13) of the sides of X.

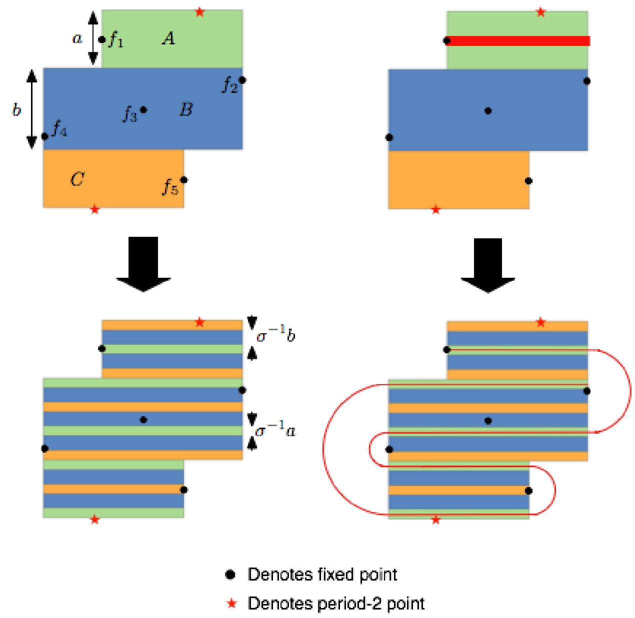

FIGURE 15. Time-1 Map in the Limit as Taffy Mass Approaches Zero.

In the image on the right, the line has been artificially extended to show the path of the region. This line also approximates a piece of the stable manifold of the fixed point f_1. This unstable manifold is a ray. The colored strips in the lower half of the figure are thinner by a factor of σ and longer by a factor of σ when we add the lengths of all strips of a given color. The stars represent a period-2 orbit whose unstable manifold include the upper and lower edges of the rectangle.

Identification on the end. Before discussing in detail the action of our 2-D taffy map, we must carefully describe the invariant domain. In order to preserve the continuity of the taffy, the vertical segments above and below each "external" fixed point (f_1, f_2, f_4, f_5 in Figure 15) must be identified. Figure 16 shows this identification. The semi-circles connect points that are identified with each other. The dots represent fixed points. We write $\hat{X}$ for this set after making these identifications.

Note that as with the well-known baker's map (Figure 4), the two-dimensional map is one-to-one except on the edges where the map is two-to-one. This reflects the fact that the outer edge of the taffy is entrained inside after a revolution of the machine.

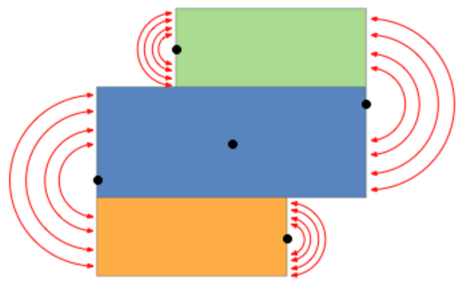

FIGURE 16. Identification of Vertical Segments Above and Below Each "External" Fixed Point.

Let F denote the time-1 map shown in Figure 15. It acts piecewise linearly on each colored region and has derivative

$$DF = \pm \begin{pmatrix} \sigma & 0 \\ 0 & \sigma^{-1} \end{pmatrix}$$

everywhere except the external fixed points. The ambiguity with respect to sign arises because, while the taffy is squeezed vertically and stretched horizontally everywhere, in some regions there is a 180° rotation and in others not. Heuristically, F stretches the region horizontally away from f_1, but "horizontally" here means following the identifications. This construction satisfied our initial goals. To our surprise, we found a further abstraction, which we discuss in section 5.

The partition. The colored partition consists of three compact rectangles (the colored rectangles in Figure 14). (An alternative partition for X is shown in Figure 18.) The six left and right ends of the partition rectangles in Figure 14 are pieces of stable manifolds of cam fixed points. The image of a rectangle (which is σ times longer than the original) will have ends on the stable manifolds. Hence, the image of a rectangle stretches entirely across a rectangle if it enters a rectangle and may stretch across several times. The top and bottom edges of each colored rectangle are all subsets of the stable manifold of the period-2 orbit indicated in Figure 15 by stars.

The transition graph (Figure 17) shows how many times each rectangle stretches across the others. The partition is a "Markov partition" because each contracting end of a rectangle maps into a contracting end of a rectangle and because the inverse of the map has the same property. The colored regions in Figure 14 represent a natural Markov partition of this map, natural because it comes directly from the drawings in Figure 3.

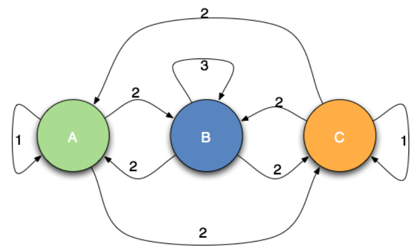

FIGURE 17. Transition Graph for 2-D Taffy Map.

This transition graph is valid for the partitions indicated by the monochrome rectangles in figures 14 and 18. The numbers with the bent arrows represent how many times the image of a region stretches across the region the arrow points to. For example, the arrows indicate that the image of region A stretches across itself once and twice across each of B and C. Figure 18 shows how the map stretches A.

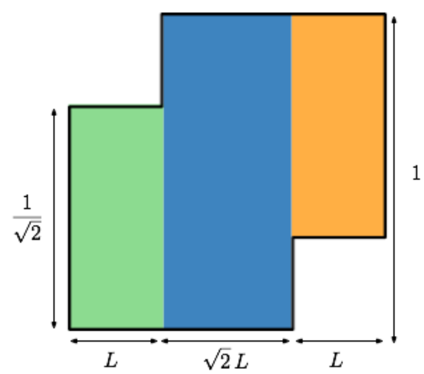

FIGURE 18. An Alternative Markov Partition.

Another partition is interesting: the rectangles that are the intersections of one rectangle in Figure 14 and one from Figure 18. There are seven such rectangles. Each rectangle maps across itself and the others either zero or one time, thereby avoiding the 2's and 3's in Figure 17.

Figure 18 displays an alternative Markov partition for the dynamics. The one-dimensional map has a Markov partition of $[0, 1]$ consisting of the three intervals shown in Figure 12. The middle interval maps across itself three times. There is also a seven-interval Markov partition consisting of the seven maximal intervals on which the 1-D map T is monotonic (see

Figure 11). It has the desirable property that each interval maps across each partition interval at most once.

A new space $\hat{\hat{X}}$. We now identify any two points on the boundary of X that can be mapped onto each other by a sequence of rotations about cam points and their images, and we call the resulting space $\hat{\hat{X}}$.

5. Tiling the Plane

The four fixed points on the edges of X came from the cams so we call them *cam* fixed points (Figure 15).

One way to understand the geometry near any of the four cam fixed points is to rotate the block about the fixed points as shown in Figure 19. Each additional block is an additional representation of the original block and not an increase in the size of the region. Points q_1 and q_2 in the larger region are identified if each is carried onto the other under a 180° rotation of the plane about a cam fixed point. In $\hat{X}$, the top and bottom edges of the block have been distinct. In $\hat{\hat{X}}$, they are identified.

In Figure 19, the dots represent the rotation fixed points. These points represent the cams in the original taffy map of Figure 2. The crosses represent the other fixed points. The stars represent period two points. Note that the unstable manifold of each of these rotation fixed points is a horizontal ray, not a two-sided manifold as holds for hyperbolic fixed points. Also note that the stable manifold of each of those points is a vertical line in X, but since the part above the fixed point is identified with the part below, the stable manifold is also a ray in $\hat{X}$.

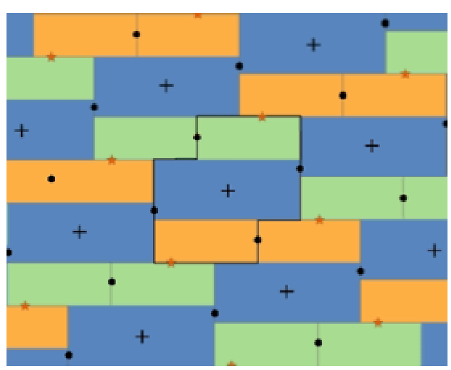

Figure 19. Tiling of the Plane with Copies of the Taffy Set X. [Click on image.]

Composition of an even number of rotations is a translation. There are two points denoted by stars in Figure 15 that are a period-2 orbit. In $\hat{\hat{X}}$, they are identified, becoming a sixth fixed point, a second non-cam fixed point. By identifying the top edges in this fashion, the map is now one-to-one on the new space. The identifications effectively sew up the region and remove the boundary. The map on the block can now be represented as a linear map on the plane when we allow some points to map into a different copy of the block. We apply the map

$$T = -1 \cdot \begin{pmatrix} \sigma & 0 \\ 0 & \sigma^{-1} \end{pmatrix}$$

to the plane. The taffy is locally stretched horizontally by a factor σ and contracted vertically by σ^{-1}. The factor of -1 reflects the behavior of the animation in Figure 2 where the taffy flips over in the course of the motion. In Figure 20, we see the "continuous motion" application of this map to our taffy tiling. Making this map continuous is artificial but it helps illustrate which strips map to which strips. Because the entries in T are negative, we must add a 180° flip at the end of the animation. Vertical sides map into vertical sides.

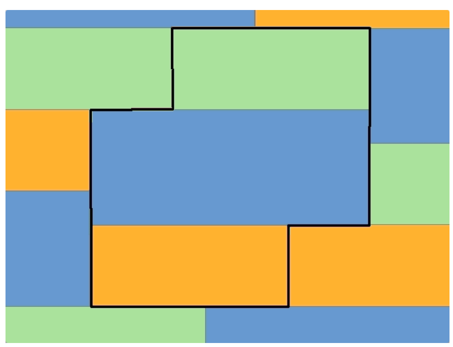

FIGURE 20. "Continuous Motion" Application of T to the Tiled Plane. [Click on image.]

Now we can understand the dynamics by applying T in the plane and then rotating them back into the fundamental domain according to the identifications.

Change in coordinates. For the rest of this paper, we will use a different coordinate system. We change to coordinates with the lines $\overline{f_3 f_2}$ and $\overline{f_3 f_1}$ as axes (see Figure 15). In these coordinates, the map has matrix

$$\hat{T} = \begin{pmatrix} -5 & 2 \\ 2 & -1 \end{pmatrix}.$$

In the new coordinate system, the four cam points of the basic block are $(0, \pm 1)$ and $(\pm 1, 0)$. Their images under multiple rotations are

$$\mathbb{L} = \left\{ (n, m) \in \mathbb{Z}^2 \mid n + m \text{is odd} \right\}.$$

Fundamental domains. By *fundamental domain*, we mean a compact region X_1 in the plane such that each point of our space $\hat{\hat{X}}$ has at least one representative in X_1 and, if a point has multiple representatives, all are on the boundary of X_1. To prevent confusion, we refer to X as the (original) fundamental domain and $\hat{X}$ as the fundamental domain with the segments on either side of exterior fixed points identified. Figure 21 shows that an alternative fundamental domain is the square in the plane given by $X_0 = \{(x, y) : |x|, |y| \leq 1\}$. Notice that all four corners represent the same point, the sixth fixed point.

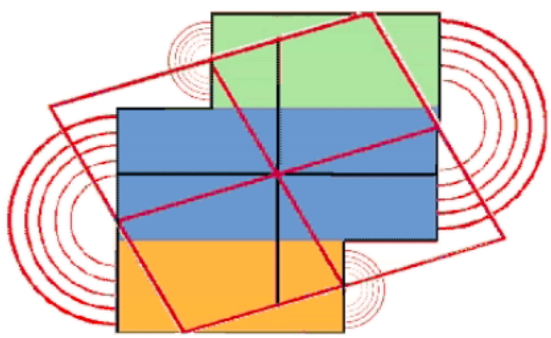

FIGURE 21. Alteration of the Fundamental Domain. [Click on image.]

Any piece of the original fundamental domain can be replaced by an equivalent piece in the plane. We can change X into the parallelogram X_0 by four such substitutions, substituting pieces inside the parallelogram for pieces of X that are outside it. The animation in Figure 21 shows how the original fundamental domain X can be changed to X_0 by a different selection of the boundary. The four corner points of X_0 are the same point of $\hat{\hat{X}}$, a sixth fixed point. The final frame is aligned so that the new coordinate axes connect rotation points. The parallelogram X_0 can be viewed as a square since the two differ only by equivalent metrics. Section 7 takes the square one step further.

We leave it to the reader to show that the map is continuous on all of these representations. A key point in showing continuity is that if two points are equivalent in one of these representations, they always map to equivalent points.

The taffy space $\hat{\hat{X}}$ can now be seen to be a topological sphere (Figure 22).

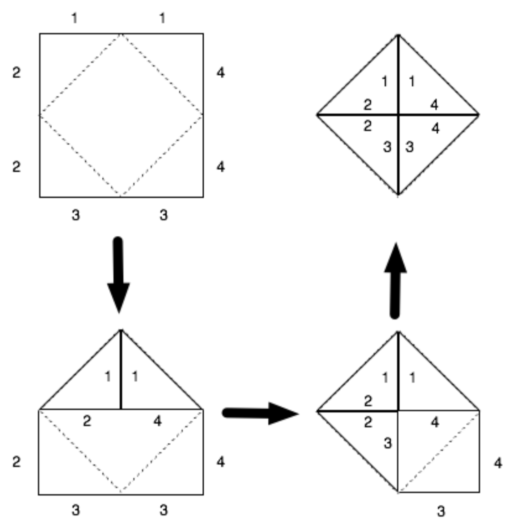

FIGURE 22. A "Square Sphere."

Dotted lines show how one might fold a square fundamental domain so that parts of edges that are identified are brought together. Through this process, we create a two-layer structure, two smaller squares that are stitched together along their edges. Such an object is a topological sphere. The four corner points in the folded version are the cam fixed points. The four corner points in the original larger square are a single fixed point.

Since the taffy space $\hat{\hat{X}}$ has a fundamental domain X_0 that is a square, we call it a "square sphere" (see Figure 22) and refer to it as $\hat{\hat{X}}$ ($\hat{X}$ is topologically equivalent to a disk and $\hat{\hat{X}}$ is topologically equivalent to a sphere).[2]

6. The Mathematics of the "Square Sphere"

This paper is written so that it will be intelligible to the mathematician or scientist who is not familiar with the literature on factor spaces $\mathbb{R}^2/G$ where G is a discrete group of isometries of $\mathbb{R}^2$. The taffy space $\hat{\hat{X}}$ is a set of equivalence classes in $\mathbb{R}^2$ defined as follows. To every point p in the plane, there corresponds a map R_p that rotates points around p, i.e., $R_p(q) = 2p - q$. We refer to such maps as "rotations." Of course, the composition of an even number of rotations is a translation. Note that $R_p(p + \delta) = p - \delta$. Notice that $R_{p_1}R_{p_2}(q) = 2(p_1 - p_2) + q$ and, more generally, we obtain an alternating sum of p_i's.

$$R_{p_1}R_{p_2}\cdots R_{p_n}(q) = 2(p_1 - p_2 + \cdots \mp p_n) \pm q$$

where "$\pm$" means "$+$" if n is even and "$-$" if n is odd and "$\mp$" means the opposite sign. Writing $s = p_1 - p_2 + \cdots \pm p_n$, we observe that $R_{p_1}\cdots R_{p_n}$ is a translation by s if n is even and is $R_s(q)$ if n is odd.

Now let $\mathbb{L} = \{(n, m) \in \mathbb{Z}^2 \mid n + m \text{ is odd}\}$. Let

$$R_{\mathbb{L}} = \{R_{(m,n)} | (m, n) \in \mathbb{L}\}$$

be the collection of rotations about points of $\mathbb{L}$ and let $G = \langle R_{\mathbb{L}} \rangle$ be the group of isometries generated by these rotations. We write $a \sim b$ if $b = \mathbf{g}a$ for some $\mathbf{g} \in G$ and say "a is equivalent to b." This means $a \sim b$ if and only if a can be mapped to b by a finite sequence of rotations about rotation points. The *taffy surface* Z or *square sphere* is defined to be $\mathbb{R}^2/G$, the set of the corresponding equivalence classes of points.

[2]When we began modeling the taffy-pulling process, we did not foresee that there is a choice of the length parameters S and L that makes all the slopes of the one-dimensional map the same. Our choice of this regime has the unforeseen consequence of making the derivative of the two-dimensional process everywhere (except at the cams) the same, up to a change in sign. Other choices of S and L appear to result in an interesting class of area-preserving homeomorphisms on the sphere that are only piecewise linear. In 2006, another piecewise linear pseudo-Anosov map appeared in the literature (though on a torus rather than a sphere) [9]. Kazu Aihara has discussed chaos on Japanese television, showing a different taffy machine that has three cams. That machine also has a representation as a one-dimensional map that is continuous and piecewise linear, analogous to Figure 10, but we have not found a constant slope version analogous to Figure 11. Had we started with Aihara's taffy machine, this paper would have been quite different.

Theorem 6.1 (Square Sphere)**.** *Let* $Z = \mathbb{R}^2/G$ *and*

$$\mathbf{M} = \begin{pmatrix} a & b \\ c & d \end{pmatrix} : \mathbb{R}^2 \to \mathbb{R}^2$$

be a linear map on the plane. Then $\mathbf{M}$ *induces a continuous map on* Z *if and only if* $a, b, c, d \in \mathbb{Z}$ *and* $a + c$ *and* $b + d$ *are both odd.*

Before proving this result we give some preliminary results.

Let W be the union of lines $\{(x, y) \mid \text{either } x \text{ or } y \text{ is an odd integer}\}$. The components of $\mathbb{R}^2 \setminus W$ are open squares; the centers of the sides of the squares are the points of $\mathbb{L}$. The rotations in $\mathbb{L}$ map squares to squares, i.e., $\mathbb{R}^2 \setminus W$ to itself.

Lemma 6.2. *Let* $p_1, p_2 \in \mathbb{R}^2$*. If* $p_1 \sim p_2$ *and both are in the same component of* $\mathbb{R}^2 \setminus W$*, then* $p_1 = p_2$*.*

Proof. Let $C = \{(c, d) \mid \text{both } c \text{ and } d \text{ are even integers}\}$. Notice that C is the collection of center points of components in $\mathbb{R}^2 \setminus W$. Let

$$C_0 = \{(c, d) \in C \mid c + d \text{ is divisible by } 4\} \text{ and } C_1 = C \setminus C_0.$$

If $p_0 = (c_0, d_0)$ and $p_1 = (c_1, d_1)$ are in C_0 and C_1, respectively, then $p = (p_0 + p_1)/2 \in \mathbb{L}$ and the rotation $R_p : p_0 \mapsto p_1$ and vice versa. In particular, each rotation in $R_{\mathbb{L}}$ maps C_0 onto C_1 and C_1 onto C_0. Hence, if a point in C is mapped to itself by the composition of n maps in $R_{\mathbb{L}}$, then n is even, so the composition is a translation. Since one point is fixed, the composition is the identity. $\square$

One can prove the following lemma along the same lines.

Lemma 6.3. *If* $p = r + v$ *where* $r \in \mathbb{L}$*, then* $q \sim p$ *if and only if* q *is either* $r_1 + v$ *or* $r_1 - v$ *for some rotation point* r_1*. Furthermore, if* $||q - p|| < 1$*, then* $\frac{p+q}{2} \in \mathbb{L}$

Any point in the plane can be written in the form $(x, y) + (2m, 2n)$ where $|x| \le 1$ and $|y| \le 1$ and m and n are integers; this representation is unique if $|x| < 1$ and $|y| < 1$. The following result follows from Lemma 6.2 and Lemma 6.3.

Proposition 6.4. $(x, y) + (2m, 2n) \sim (-1)^{m+n}(x, y)$ *where* $x, y \in X_0$ *and* $m, n \in \mathbb{Z}$*. In particular, if* $|x| = 1$*, then* $(x, y) \sim (x, -y)$*, and if* $|y| = 1$*, then* $(x, y) \sim (-x, y)$*.*

Proof. $(x, y) + (2m, 2n) \sim -(x, y) + (2(m-1), 2n)$ by rotation about $(2m - 1, 2n)$. By induction, m can be decreased to 0 (or increased to 0 if $m < 0$) and so can n in a total of $|m| + |n|$ steps; $|m| + |n|$ is odd if and only if $m + n$ is. $\square$

To understand these relationships, consider the example $(1, y)$ which can be written as $(-1, y) + (2, 0)$, which, by Proposition 6.4, is equivalent to $(-1, y)$. Hence, $(1, y) \sim (1, -y)$.

Lemma 6.5. $\mathbf{M}R_p = R_{\mathbf{M}p}\mathbf{M}$ *for all linear maps* $\mathbf{M} : \mathbb{R}^2 \to \mathbb{R}^2$.

Proof.

$$\begin{aligned} R_p(q) &= 2p - q \\ \mathbf{M}R_p(q) &= 2\mathbf{M}p - \mathbf{M}q \\ &= R_{\mathbf{M}p}(\mathbf{M}q). \end{aligned}$$

□

Proof of Theorem 6.1. Notice that $\mathbf{M}(1, 0)$ and $\mathbf{M}(0, 1)$ are both in $\mathbb{L}$ if and only if the above conditions on a, b, c, and d are satisfied. More generally, they are equivalent to requiring $\mathbf{M} : \mathbb{L} \to \mathbb{L}$. We will show that $\mathbf{M}$ induces a continuous map on S if and only if $\mathbf{M}(\mathbb{L}) \subset \mathbb{L}$. From this will follow the conditions of the theorem.

Assume M induces a continuous map on S. This implies that M is well defined on S. That is, $p \sim q$ implies $\mathbf{M}p \sim \mathbf{M}q$. Let $p \in \mathbb{L}$ and choose $\delta \in \mathbb{R}^2$ with $|\delta| < \frac{1}{2||\mathbf{M}||}$. Since $(p + \delta) \sim (p - \delta)$, we have that $\mathbf{M}(p + \delta) \sim \mathbf{M}(p - \delta)$. The choice of δ implies $\mathbf{M}(p + \delta)$ and $\mathbf{M}(p - \delta)$ will be so close that, by Lemma 6.3,

$$\frac{\mathbf{M}(p + \delta) + \mathbf{M}(p - \delta)}{2} = \mathbf{M}p \in \mathbb{L}.$$

So we see that $\mathbf{M}(\mathbb{L}) \subset \mathbb{L}$.

Now suppose $\mathbf{M}(\mathbb{L}) \subset \mathbb{L}$. Assume $p \sim q$, i.e., $q = \mathbf{g}p$ for some $\mathbf{g} \in G$. By the definition of G, we have

$$\mathbf{g} = R_{q_m} R_{q_{m-1}} \cdots R_{q_1}$$

for some finite set $\{q_1, q_2, \ldots, q_m\} \subset \mathbb{L}$. Hence, we have

$$\mathbf{M}q = \mathbf{M}\, R_{q_m} R_{q_{m-1}} \cdots R_{q_1} p.$$

By repeated application of Lemma 6.5, we have

$$\mathbf{M}q = R_{\mathbf{M}q_m} R_{\mathbf{M}q_{m-1}} \cdots R_{\mathbf{M}q_1} \mathbf{M}p,$$

but now $\mathbf{M}q_i \in \mathbb{L}$ for each i so $R_{\mathbf{M}q_m} R_{\mathbf{M}q_{m-1}} \cdots R_{\mathbf{M}q_1} \in G$ and so $\mathbf{M}p$ and $\mathbf{M}q$ are equivalent under G. From this we see that $\mathbf{M}$ induces a well-defined map on S. The conclusion follows by noting that well-defined linear maps between finite dimensional vector spaces are automatically continuous. □

Consider the analog of Figure 15 shown in Figure 23.

We see that the colored regions are a natural Markov partition of the sphere. Also note that we can draw transverse foliations along the lines of

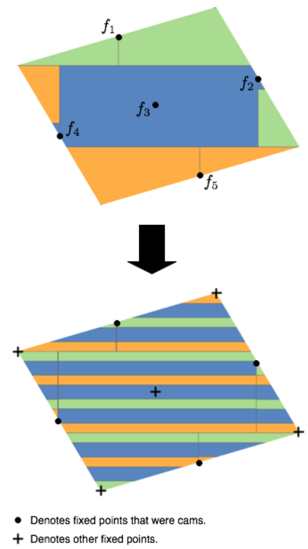

FIGURE 23. Time-1 Map $\hat{T}$ on Sphere.

stretch and shrink. We can do this everywhere except the four midpoint fixed points. At these locations our foliations have a singularity. These are known as 1-prong singularities (see [2]).

The following precise statement of the central theorem in the Thurston-Nielsen theory (see [4]) may be found in [3].

Theorem 6.6 (Thurston-Nielsen Classification Theorem)**.** *If f is a homeomorphism of a compact surface S, then f is isotopic to a homeomorphism ϕ of one of the following types:*

(i) *finite order: $\phi^n = id$ for some integer $n > 0$;*
(ii) *pseudo-Anosov: ϕ preserves a pair of transverse, measured foliations $\mathcal{F}_u$ and $\mathcal{F}_s$, and there is a $\lambda > 1$ such that ϕ stretches $\mathcal{F}_u$ by a factor λ and contracts $\mathcal{F}_s$ by a factor λ^{-1};*
(iii) *reducible: ϕ fixes a family of reducing curves and, on the complementary surfaces, ϕ satisfies (i) or (ii).*

Our taffy map on a sphere is the pseudo-Anosov representative for its class in the homeomorphisms of the sphere with four holes. For more information about pseudo-Anosov maps on a sphere with four holes, consult [7]. It is interesting to note that every map isotopic to our example has dynamics at least as complicated as our the taffy pulling machine. That is, there is a large class of dynamical systems out there that contain within them dynamics quite similar to a taffy pulling machine. In

Figure 20, horizontal lines map to horizontal lines, the unstable foliation $\mathcal{F}_u$, and vertical lines map to vertical lines, the stable foliations $\mathcal{F}_s$. In our case, $\lambda = \sigma$.

A property of our map on the plane is that the midpoint of the square maps to a midpoint of a grid square. That is, the midpoint is a regular fixed point on the sphere.

7. A Simpler Description of the Chaotic Square-Sphere Map

Consider the action of

$$\begin{pmatrix} x' \\ y' \end{pmatrix} = \overbrace{\begin{pmatrix} a & b \\ c & d \end{pmatrix}}^{M} \begin{pmatrix} x \\ y \end{pmatrix} \tag{7.1}$$

on the square X_0. The dotted parallelogram is the image of X_0 under M. Choose $m, n \in \mathbb{Z}$ so that (x', y') is in the fundamental domain $X_{m,n} = X_0 + (2m, 2n)$; that is, the center is at $(2m, 2n)$. Then

$$(x'', y'') = [(x, y) - (2m, 2n)]\,(-1)^{m+n} \in X_0 \tag{7.2}$$

and $(x'', y'') \sim (x', y')$. Notice that two adjacent fundamental domains, $X_{i,j}$ and either $X_{i+1,j}$ or $X_{i,j+1}$, have a rotation point at the midpoint of their shared boundary. We can map $X_{m,n}$ to $X_{0,0}$ (which is X_0) through a series of $m + n$ such rotations, resulting in the factor $(-1)^{m+n}$ in equation (7.2).

By Theorem 6.1, we consider only matrices with $a, b, c, d \in \mathbb{Z}$ where $a + c$ and $b + d$ are both odd. The simplest such linear maps are I and $-I$. Another example is the 90° rotation

$$\begin{pmatrix} 0 & 1 \\ -1 & 0 \end{pmatrix}$$

in which the four rotation points form a period-4 orbit.

Note that

$$\begin{pmatrix} 2 & 1 \\ -1 & 0 \end{pmatrix}$$

has both eigenvalues equal to 1. Perhaps the simplest chaotic example of a square sphere map is given by the symmetric matrix

$$\mathbf{M} = \begin{pmatrix} 2 & 1 \\ 1 & 0 \end{pmatrix}$$

which has eigenvalues $1 \pm \sqrt{2}$ (Figure 24).

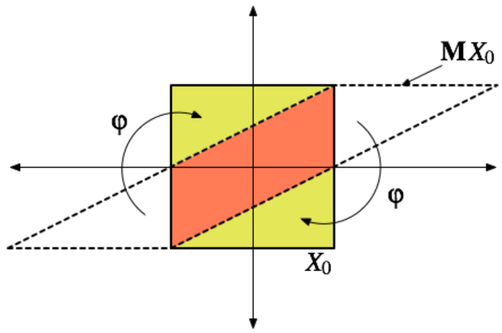

FIGURE 24. A Simple Square Sphere Map.

The matrix M (equation (7.1)) with $a = 2$ and $b = c = 1$, and $d = 0$ maps $X_0 = [-1, 1] \times [-1, 1]$ to a parallelogram, preserving area since $\det M = -1$. The arrows show how ϕ (equation 5.1) maps the parts of MX_0 back into X_0. $\hat{X}_0$ is the colored square.

Note the determinant is -1 and the rotation points consist of a period-4 orbit since $\mathbf{M}(0, 1) = (0, 1)$ and $\mathbf{M}(1, 0) = (2, 1)$, which is equivalent to $(0, -1)$, as may be seen by rotating it about $(1, 0)$. Clearly, two more applications of $\mathbf{M}$ on $\hat{\hat{X}}$ bring $(0, -1)$ back to $(0, 1)$. Note that $\mathbf{M}$ has eigenvector $(1, \sqrt{2} - 1)$ for eigenvalue $1 + \sqrt{2}$, so the unstable manifolds have slope $\sqrt{2} - 1$.

8. Viewing Classical Maps through Animation

R. V. Plykin [10] created the first diffeomorphism in the plane with a chaotic hyperbolic attractor. Understanding it has required considerable study, so Newhouse (see [11]) suggested a simpler process. The key simplification Newhouse provided was to replace the three fixed points with a period-3 orbit.

In this section, we display the Plykin map (Figure 25) and the Newhouse map (Figure 26) through animation. These are discrete time maps but, by making the map the end of an animation, it becomes easier to see what the map is. These are not drawn to scale.

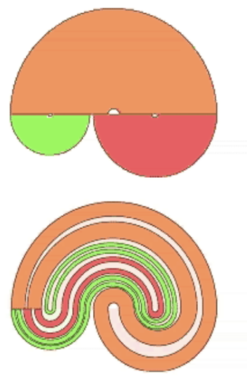

FIGURE 25. Plykin Map. [Click on image.]

FIGURE 26. Newhouse Map. [Click on image.]

This Newhouse map is constructed around a period-3 orbit, $p_1 \to p_2 \to p_3 \to p_1$ which is a repeller, though that is not obvious in the animation.

In Figure 27, three iterations yield an image of the square having eight vertical strips.

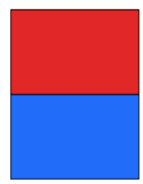

Figure 27. Skinny Baker's Map. [Click on image.]

Appendix A. A Simpler Chaotic "Triangle-Sphere" Map

A three-cam taffy-pulling process can yield the block system in Figure 28. The block will be stretched by a factor of $1/x$ in the horizontal direction. The coloring represents a Markov partition. The three dots are special points that will constitute a period-3 orbit in the next figure. In order to have the stretching be Markov, we require $1/x = 1 + x$, which implies $x = \left(\sqrt{5} - 1\right)/2$. We leave it to the reader to construct the analog of Figure 13 which begins with a curvilinear region.

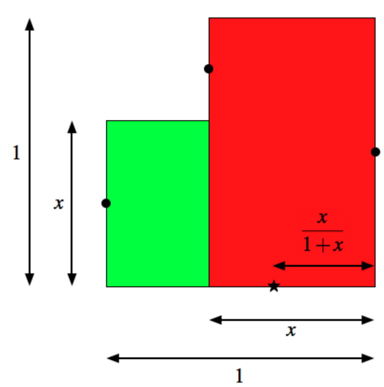

Figure 28. Simpler "Taffy-like" Map.

This will be the fundamental domain for this simpler "taffy-like" transformation. The set in the figure is made into a disk by identifying the segments as shown in Figure 29. The shape is stretched horizontally by a factor $1/x$, then the smaller rectangle of the shape is removed and placed on top. The entire shape is then flipped around its center.

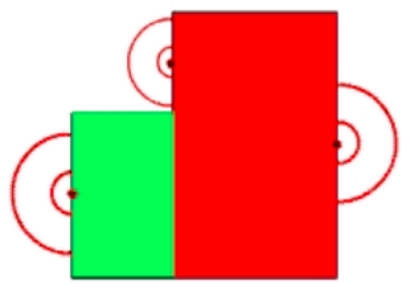

FIGURE 29. Simpler Chaotic 3-Cam Taffy-pulling Process. [Click on image.]

Figure 30 shows how the fundamental region can be changed into a triangle. Having a triangle sphere came as a surprise to the authors.

This process can be seen to be continuous and, in fact, reformulated in much the same way the 2-D taffy-pulling process was in section 6. The process just described implies the existence of a fixed point on the bottom edge of the shape (the bottom edge is mapped onto itself). Place the shape in a coordinate frame with that fixed point as the origin. Then apply the map

$$\mathbf{K} = \begin{pmatrix} -\frac{1}{x} & 0 \\ 0 & x \end{pmatrix}.$$

This both flips and stretches the shape. If we force the stretching to follow the identification, we see that the map is continuous.

Tiling the plane. We tile with the shape shown in Figure 28 as we did in section 5. Rotated copies fill the plane. We find we can choose a fundamental domain that is bounded by three line segments, each having a

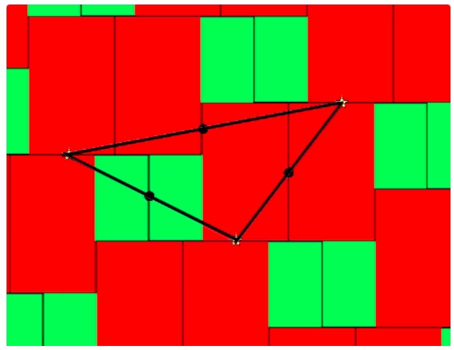

FIGURE 30. Tiling and Transformation of the 3-Cam Process Fundamental Domain into a "Triangle-Sphere." [Click on image.]

rotation point at its center. The three vertices of the triangle are the same point when identified and constitute a fixed point under the dynamics. We chose coordinates so that the lines joining the star (the fixed point) to the two points of the period-3 orbit on the left and right are axes. We see that the fundamental domain can be considered as a triangle and, in the new coordinate frame, the matrix for the operation is

$$\tilde{\mathbf{K}} = \begin{pmatrix} 0 & 1 \\ 1 & -1 \end{pmatrix}.$$

A note on the creation of animations

All the images in this paper and the key frames in the animations (except for Figure 8, which involved a simple numerical manipulation of vector graphics) were drawn by hand (so to speak) with a combination of Adobe Illustrator, Macromedia Fireworks, Macromedia Freehand, and Omnigraffle. In principle they could be drawn with any software package that supports Bezier Curves (e.g., xFig or Gimp). All animations were created using Macromedia Director software. At the time this project was begun this was the best software package available on a Mac that had a full internal scripting language. Shortly thereafter, however, Macromedia introduced ActionScript for Flash. In the future Halbert will use Flash. The software is less expensive (student version) and the output Flash is more broadly viewable, though Flash does not have the flexibility of Director. Animations can also be constructed (with a little more work) using the ImageMagick software suite. ImageMagick is free software available for most platforms.

References

[1] Kathleen T. Alligood, Tim D. Sauer, and James A. Yorke, *Chaos: An Introduction to Dynamical Systems*. Textbooks in Mathematical Sciences. New York: Springer-Verlag, 1997.

[2] M. Bestvina and M. Handel, *Train-tracks for surface homeomorphisms*, Topology **34** (1995), no. 1, 109–140.

[3] Philip L. Boyland, Mark A. Stremler, and Hassan Aref, *Topological fluid mechanics of point vortex motions*, Phys. D **175** (2003), no. 1-2, 69–95.

[4] Andrew J. Casson and Steven A. Bleiler, *Automorphisms of Surfaces after Nielsen and Thurston*. London Mathematical Society Student Texts, 9. Cambridge: Cambridge University Press, 1988.

[5] Yves Coudene, *Pictures of hyperbolic dynamical systems*, Notices Amer. Math. Soc. **53** (2006), no. 1, 8–13.

[6] A. Lasota and James A. Yorke, *On the existence of invariant measures for piecewise monotonic transformations*, Trans. Amer. Math. Soc. **186** (1973), 481–488 (1974).

[7] Jaume Llibre and Robert S. MacKay, *Pseudo-Anosov homeomorphisms on a sphere with four punctures have all periods*, Math. Proc. Cambridge Philos. Soc. **112** (1992), no. 3, 539–549.

[8] R. S. MacKay, *Complicated dynamics from simple topological hypotheses*, in Topological Methods in the Physical Sciences (London, 2000). Ed. V. I. Arnold, J. W. Bruce, H. K. Moffatt, and R. B. Pelz. R. Soc. Lond. Philos. Trans. Ser. A Math. Phys. Eng. Sci., 359, (2001), (no. 1784). 1479–1496.

[9] ———, *Cerbelli and Giona's map is pseudo-Anosov and nine consequences*, J. Nonlinear Sci. **16** (2006), no. 4, 415–434.

[10] R. V. Plykin, *Sources and sinks of A-diffeomorphisms of surfaces* (Russian), Mat. Sb. (N.S.) **94(136)** (1974), 243–264, 336.

[11] Clark Robinson, *Dynamical Systems: Stability, Symbolic Dynamics, and Chaos*. 2nd ed. Studies in Advanced Mathematics. Boca Raton, FL: CRC Press, 1999.

(Halbert)
E-mail address: jthalbert@gmail.com

(Yorke) University of Maryland; College Park, Maryland 20742
E-mail address: yorke@umd.edu